Stott, JJ and Redish, AD. 2014. A functional difference in information processing between orbitofrontal cortex and ventral striatum during decision-making behavior. *Phil. Trans. R. Soc. B.* **369** doi: 10.1098/rstb.2013.0472

Supplemental Figures

Figure S1*. Behavior on the spatial adjusting delay-discounting task***.** Predicted behavior for individual sessions on the spatial adjusting delay-discounting task. **(a)** In this example, the initial delay was much higher than the animal's preferred delay. During the first few laps, the rat alternated between choices, likely to gather information about which side was delayed and the duration of the initial adjusting delay (exploration, green). Then, laps were made predominantly to the non-delayed side in order to bring the adjusting delay closer to the animal's preferred delay (titration phase, blue). Once the subjective value of both sides was roughly equal, the animal alternated sides in order to keep the adjusting delay at its indifference point (alternation phase, orange). **(b)** Example session in which the initial delay was lower than the preferred delay. In this case, the animal favored the delayed side in order to raise the adjusting delay and bring it up to the level of his indifference point. **(c)** Behavioral data from all rats (n = 6 rats, 164 sessions) showing the average trajectory of the adjusting delay across laps within the session. In the center panel, shading represents the percentage of sessions in which the rat experienced a particular adjusting delay on a given lap. Darker shading indicates higher probabilities. Note that the sampled adjusting delays begin broadly over the entire distribution of delays from 1 to 30, but over time the animals move the adjusting delay steadily toward a preferred delay of about 5 seconds by the end of the session. The histograms on the left and right show the distribution of initial and final delays (averaged over the last 20 laps), respectively. Red indicates that the left feeder was the delayed feeder on that day, and blue indicates that the right feeder was the delayed feeder on that day. The distribution of initial delays is flat, as they were chosen by the experimenter to evenly account for all of the delays from 1 to 30. The distribution of final delays was a roughly normal distribution, centered at 5-6 seconds.

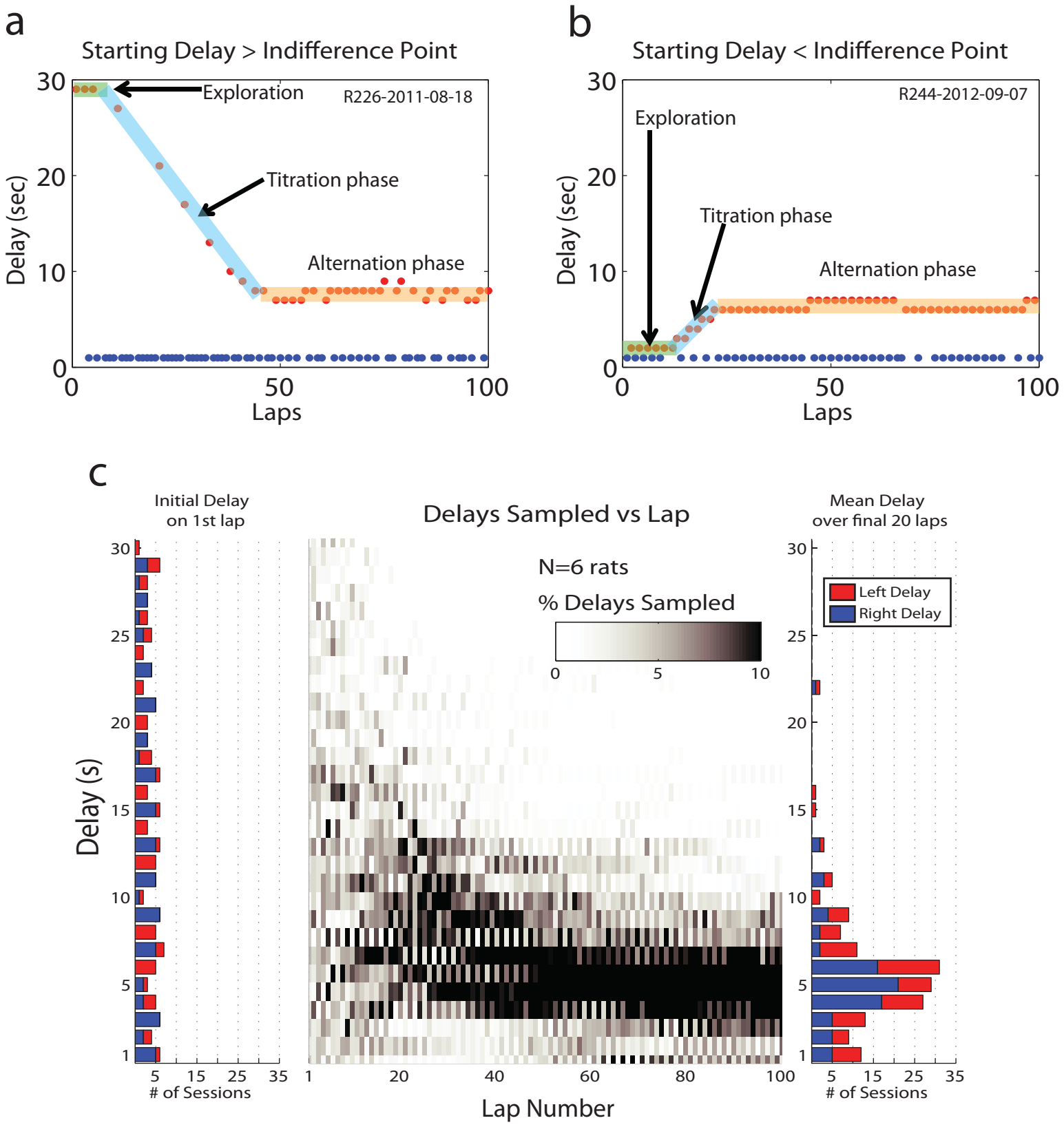
a
Starting Delay > Indifference Point
Exploration
R226-2011-08-18
Titration phase
Alternation phase
Delay (sec)
Laps
b
Starting Delay < Indifference Point
R244-2012-09-07
Exploration
Titration phase
Alternation phase
Delay (sec)
Laps
c
Initial Delay
on 1st lap
Delays Sampled vs Lap
N=6 rats
% Delays Sampled
Mean Delay
over final 20 laps
Left Delay
Right Delay
Delay (s)
# of Sessions
Lap Number
# of Sessions

Figure S2. *Histology*. **(a)** Final positions of OFC tetrodes as determined by visual inspection of tetrodes tracks and gliosis marks. Anatomical drawings are from [36]. All OFC tetrodes fell within the lateral orbital and ventral orbital cortices. OFC histology for R224 was unavailable due to a technical error during brain slicing. However, analysis results for R224 matched those of the other rats. Tetrode endpoints for R214 entered into piriform cortex. Only five cells were recorded in vStr for R214. Therefore, R214's electrophysiological data was not used for analysis, and his tetrode positions are not shown here. **(b)** Final positions of vStr tetrodes. All tetrodes (with one exception) were located within vStr or ventral caudate/putamen. Most tetrodes fell within the nucleus accumbens core, with a few in the more lateral aspect of nucleus accumbens shell.

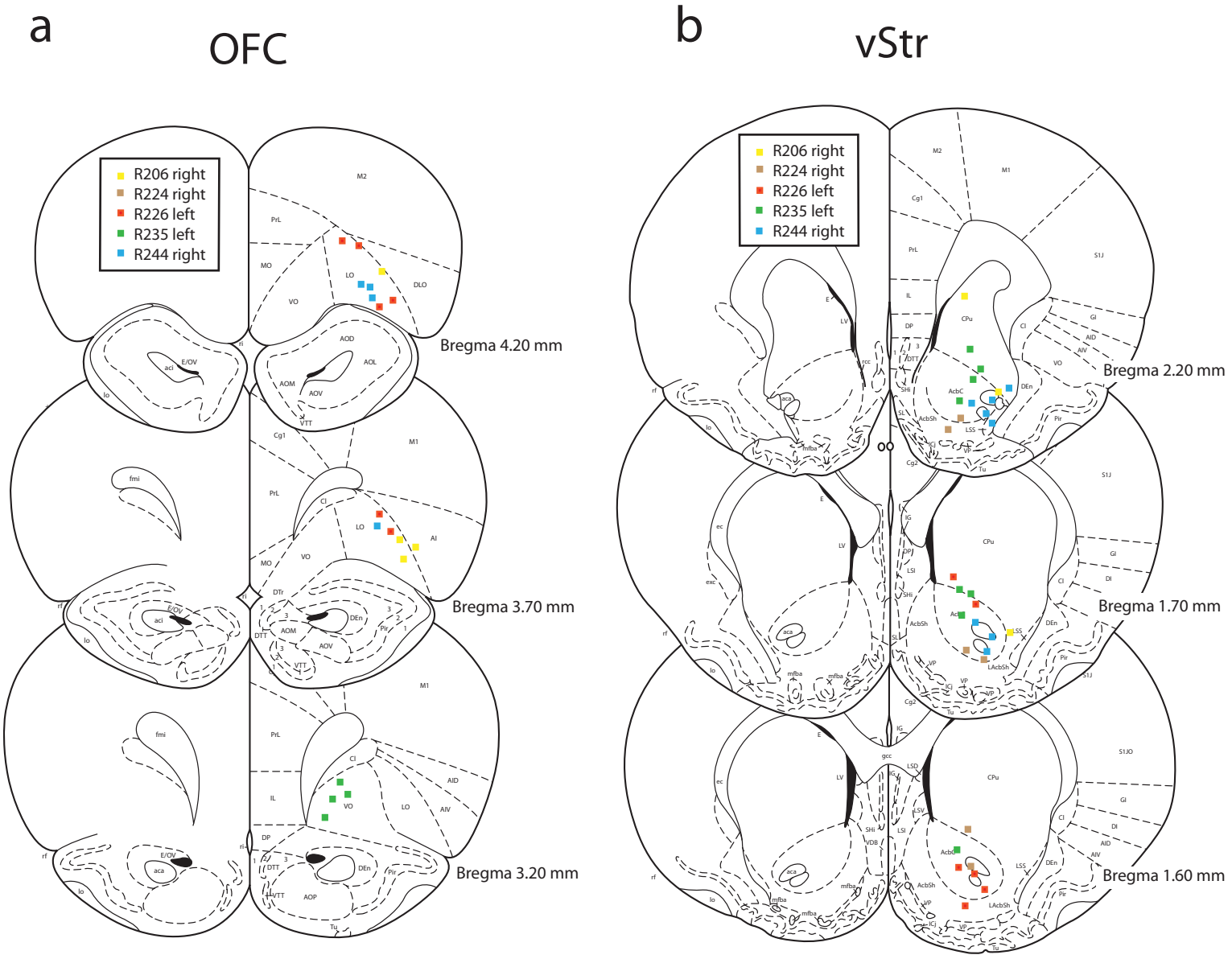
a
OFC
R206 right
R224 right
R226 left
R235 left
R244 right
Bregma 4.20 mm
Bregma 3.70 mm
Bregma 3.20 mm
b
vStr
R206 right
R224 right
R226 left
R235 left
R244 right
Bregma 2.20 mm
Bregma 1.70 mm
Bregma 1.60 mm

Figure S3. *Schematic diagram of procedure for calculating z-scores.* This data was taken from session R235-2012-01-08. For each neuron, the responses to reward during the response window (0-4 s after feeder fire) at either of the feeders are not a single number, but a distribution. In this session, the rat visited the right side feeder 48 times, and the spike raster and distribution of firing rates is shown in **(e)**. We took the average of that distribution to get an average firing rate for that cell to the right feeder (17.3 spikes/s). We next calculated a comparison distribution of firing rates for the same cell during the same window (0-4 s after feeder fire), but taken at random times during the session. Importantly, we used the same number of samples for the comparison distribution as the rat actually experienced at the right feeder; namely, 48. We then took the average of that comparison distribution to get an average firing rate.

Any one sample of 48 random times within the session could yield uncommonly low or high average values compared to the overall baseline firing rate for that cell (which was 4.02Hz)—exemplified in panels **(b)** and **(c)**, respectively. Therefore, we repeated the process 500 times to get a distribution—the bootstrap distribution (shown in panel **(d)**, although this particular example only contains 100 iterations)—which gives us a valid estimate of the distribution of firing rates from that cell when it is sampled 48 times at random. A sample taken from the middle of the bootstrap distribution, shown in panel **(a)**, lines up very well with the true baseline firing rate of that cell (4.02 Hz). The key feature of this approach is that we perform the same operation to generate the bootstrap distribution (and its attendant mean and standard deviation) as we did to find the reward response for the given cell. Separate bootstrap distributions are created for the left and right feeders, as well as for both feeders taken together. For this particular neuron, it had an average firing rate for the right feeder of 17.3 spikes/s, giving it a z-score of 16.7, compared to the bootstrap distribution—red line in **(d)**.

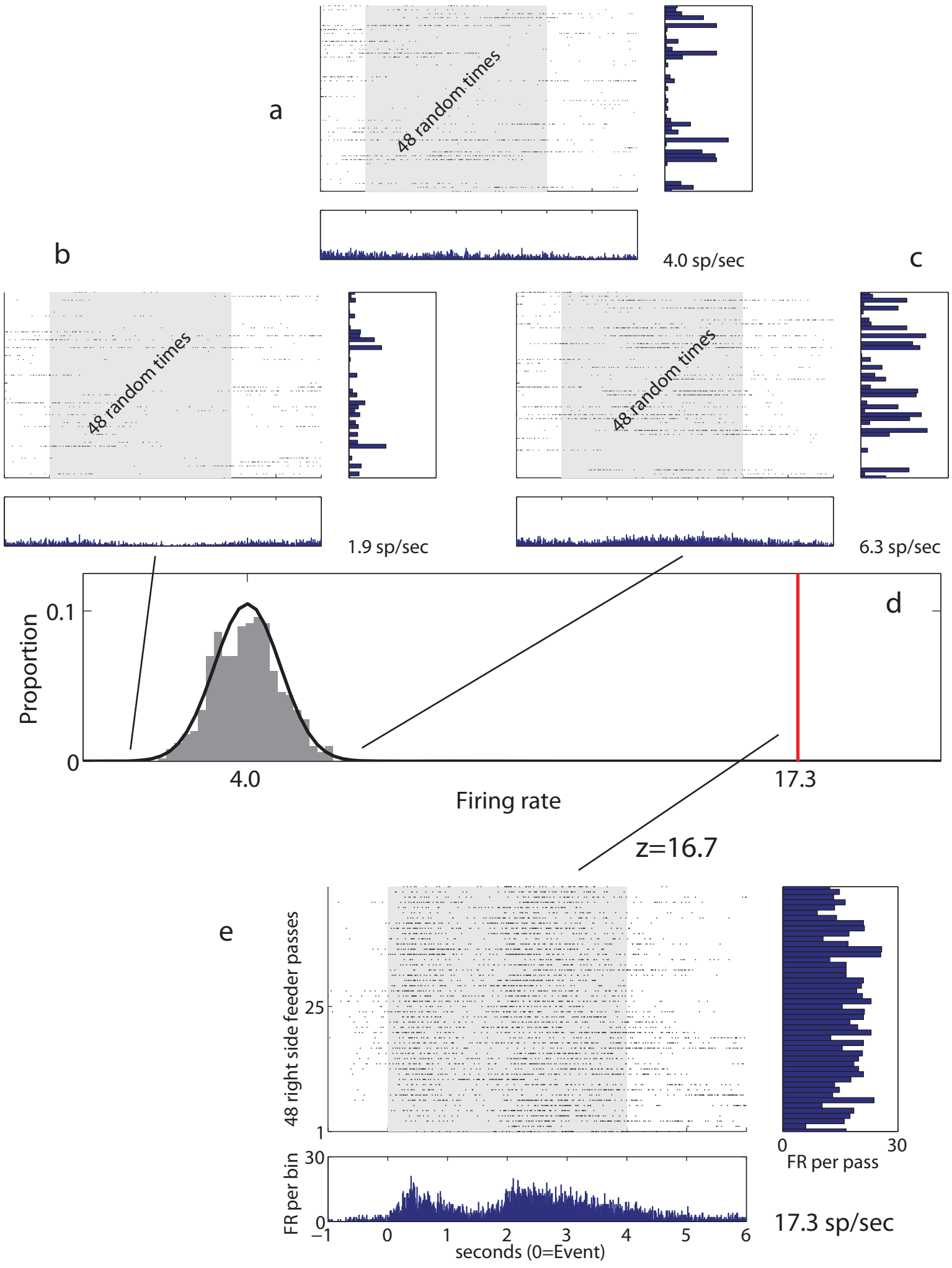
a
48 random times
4.0 sp/sec
b
48 random times
1.9 sp/sec
c
48 random times
6.3 sp/sec
d
Proportion
0.1
0
4.0
17.3
Firing rate
z=16.7
e
48 right side feeder passes
25
1
FR per bin
30
0
−1
0
1
2
3
4
5
6
seconds (0=Event)
0
30
FR per pass
17.3 sp/sec

Figure S4. *Example VTE events.* Each of the four plots shows individual behavioral examples taken from one recording session for R226. Position data from all laps are plotted in the background in grey. Over the course of a session, the rat traced out two broad curving trajectories through the choice point (one to the left, one to the right). Individual laps of interest are plotted in color. Warmer colors correspond to higher curvature values. The maximum curvature value (maxC) for the highlighted laps are shown at left in each plot. Laps were classified as VTE laps when the maximum curvature was >2. **(a)** and **(b)** show non-VTE examples of left and right passes through the choice point, respectively. The MidPoint for each lap, defined as the halfway point of the trajectory, are indicated by arrows pointing to the white asterisks. **(c)** and **(d)** show VTE examples of left and right passes through the choice point, respectively. Arrows point to the white asterisks, which indicate the start of the "TurnAround" for each VTE event.

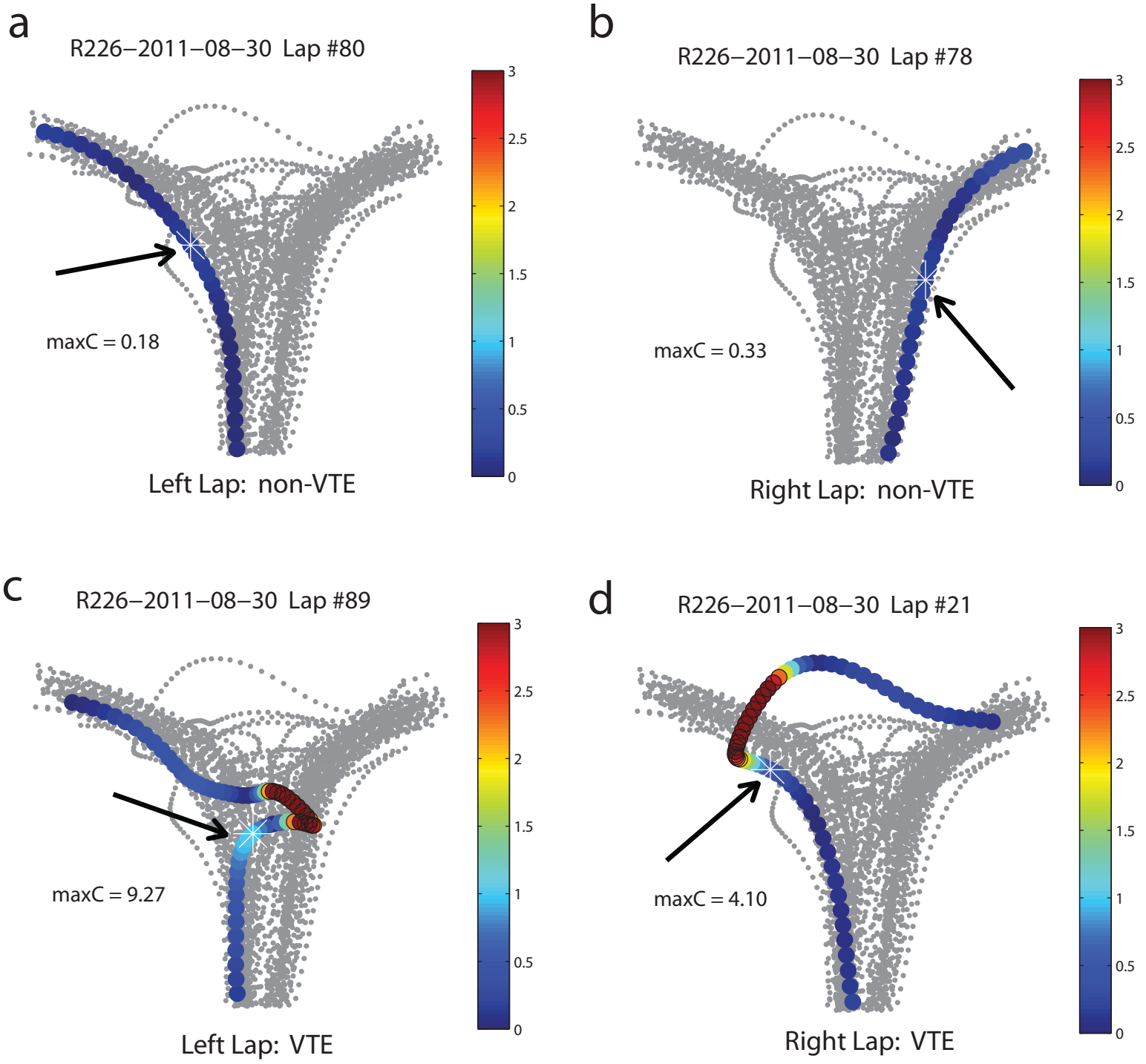
a
R226–2011–08–30 Lap #80
maxC = 0.18
Left Lap: non-VTE
b
R226–2011–08–30 Lap #78
maxC = 0.33
Right Lap: non-VTE
c
R226–2011–08–30 Lap #89
maxC = 9.27
Left Lap: VTE
d
R226–2011–08–30 Lap #21
maxC = 4.10
Right Lap: VTE
3
2.5
2
1.5
1
0.5
0

Figure S5. *Heat/Line plot showing raw firing rate data around reward receipt.* The heatmap in the middle of each plot shows the firing rate response of all neurons within a brain structure during the time window of -2 to 5 sec around reward delivery. The top row **(a,b)** shows the response to both feeders combined. The middle row **(c,d)** shows the response to the large feeder only. And the bottom row **(e,f)** shows the response to the small feeder only. These firing rate responses are normalized to the cell's maximum firing rate (range of 0 to 1) and they are ordered vertically by the z-score that defined each cell's reward response to both feeders (high z-scores at top, descending). The reward response window is marked by white lines. At right in each plot is the z-score for each neuron to the feeder or feeders specific to that plot. The z-scores are aligned to those from the top panel (sorted z-scores for both feeders), and therefore do not appear as a uniform line, as on the top panel.

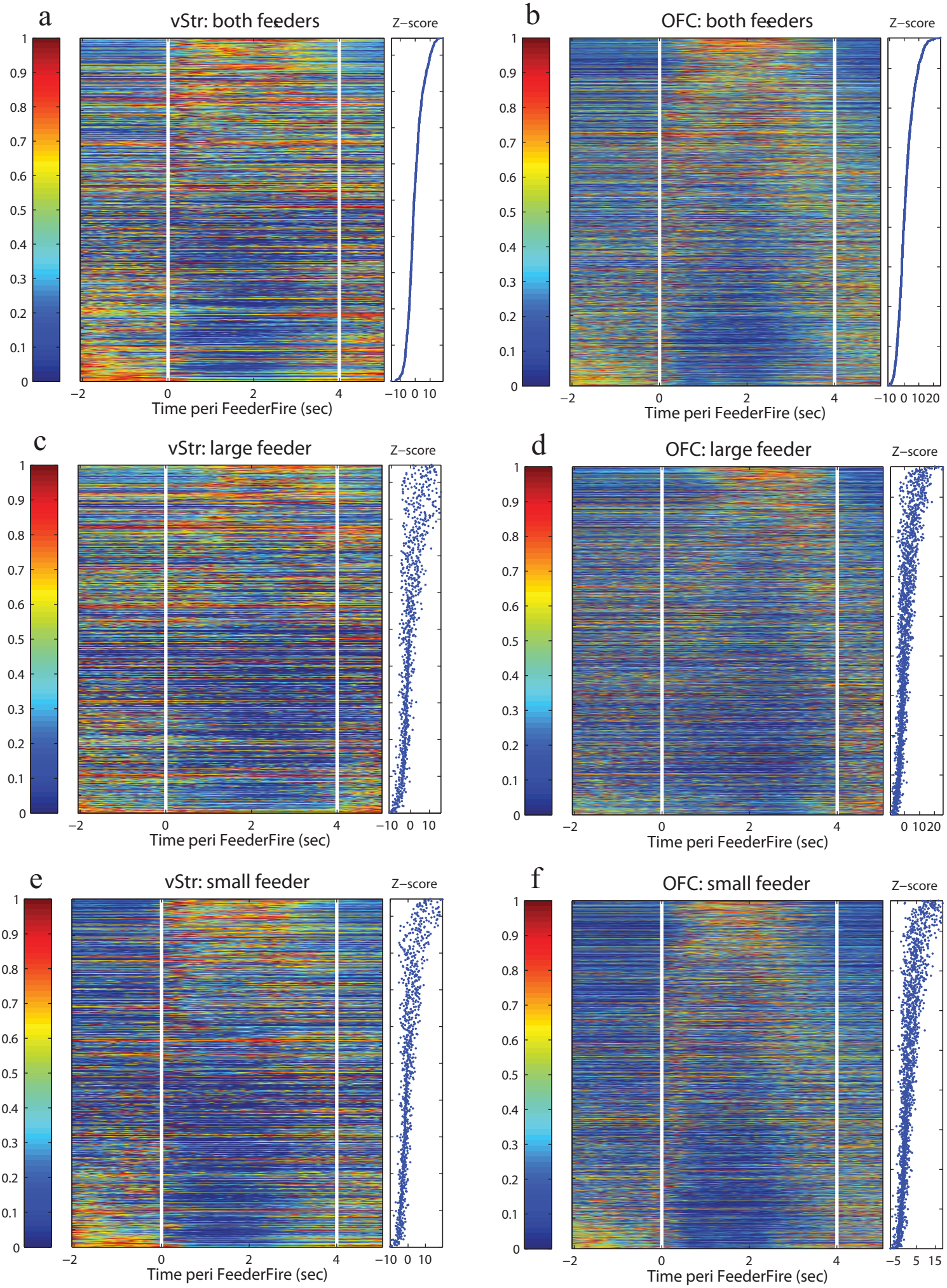
a
vStr: both feeders
Z–score
b
OFC: both feeders
Z–score
c
vStr: large feeder
Z–score
d
OFC: large feeder
Z–score
e
vStr: small feeder
Z–score
f
OFC: small feeder
Z–score
Time peri FeederFire (sec)

Figure S6. *Increased decoding in vStr during VTE events: lap-based measure.* For each session with >5 cells in vStr and >5 cells in OFC (n=85 sessions), we calculated the average decoding for VTE laps and for non-VTE laps across all laps grouped together. Lines represent the average across laps, treating laps as independent samples, with error bars representing the standard error (SEM). **(a)** Average feeder site decoding for vStr. VTE laps (n=1066) are aligned to TurnAround and non-VTE laps (n=7371) are aligned to the MidPoint of the choice point trajectory (see Methods and Fig. S4). VTE laps are shown in blue and non-VTE laps in black. We performed a paired sample t-test (right-tailed) for each time bin, testing the hypothesis that the value for VTE *pFeeders* was greater than non-VTE *pFeeders*. We applied a Bonferonni correction for 17 time bins and two conditions (VTE vs. non-VTE) for *alpha*=0.0015. P-values are shown directly below each time bin in both (a) and (b). Time bins where VTE was significantly (Bonferroni corrected) greater than non-VTE are indicated by blue and pink shading, for vStr and OFC, respectively. *pFeeders* was significantly higher in vStr prior to the time of TurnAround (time bins 7 & 8). **(b)** Average feeder site decoding for OFC. VTE laps (n=1066) are shown in red and non-VTE laps (n=7371) in black. Statistical analysis as in (a). Decoding was significantly higher on VTE laps than on non-VTE laps, but largely only after the time of TurnAround.

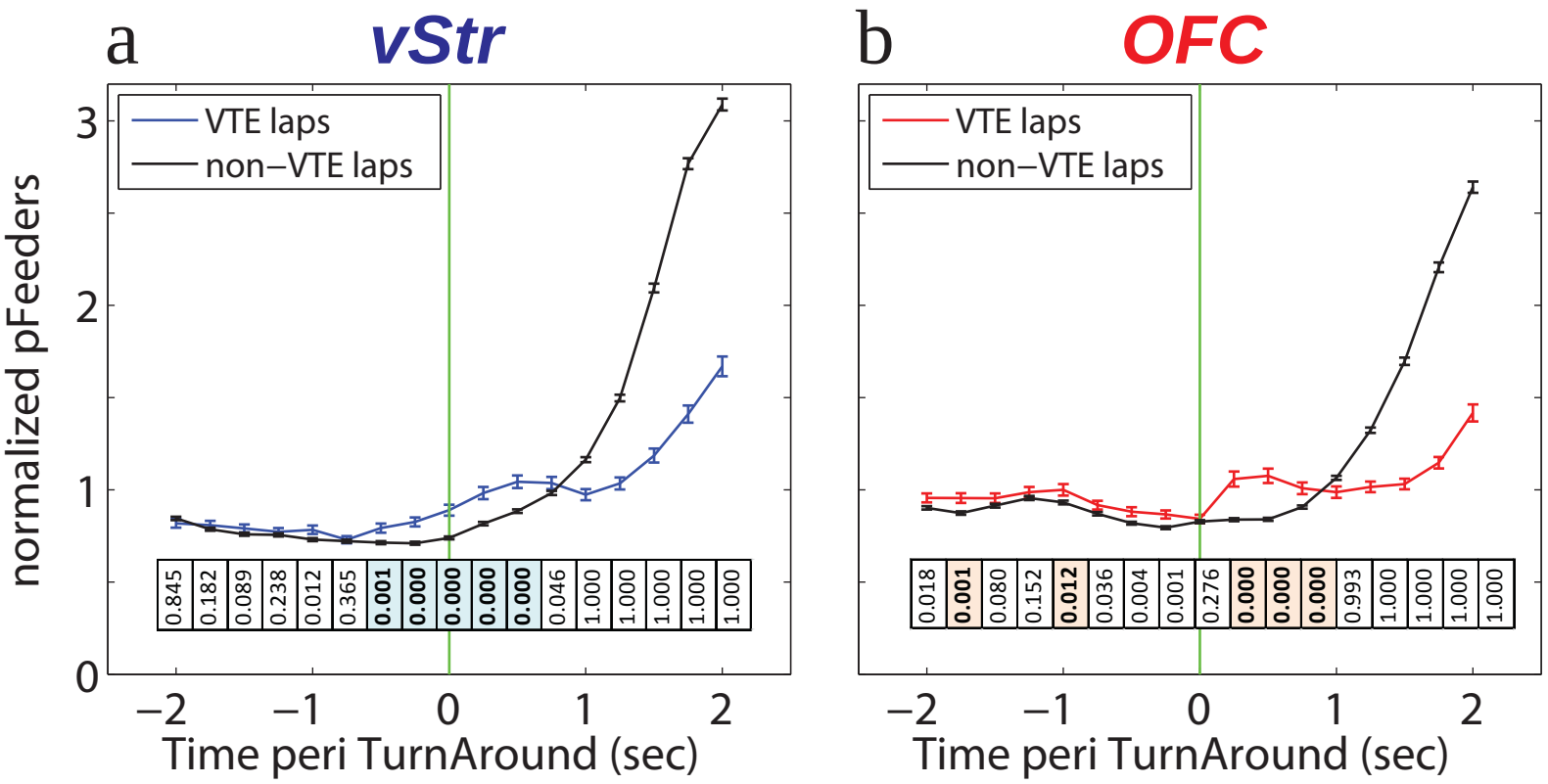
a
vStr
b
OFC
VTE laps
non–VTE laps
normalized pFeeders
Time peri TurnAround (sec)
0.845 0.182 0.089 0.238 0.012 0.365 0.001 0.000 0.000 0.000 0.000 0.046 1.000 1.000 1.000 1.000 1.000
0.018 0.001 0.080 0.152 0.012 0.036 0.004 0.001 0.276 0.000 0.000 0.000 0.993 1.000 1.000 1.000 1.000

Figure S7. *Separate feeder site representations during choice: lap-based measure.* Decoding values were averaged across laps, as in Figure S6. Lines represent the average across laps, treating laps as independent samples, with error bars representing the standard error (SEM). **(a)** Decoding to the chosen feeder site minus decoding to the unchosen feeder site for non-VTE laps (n=7371). The green line marks the MidPoint time. Values above the dotted line indicate greater decoding to the chosen feeder site. T-tests were performed on each time bin, with the null hypothesis that *pFeeder* was not significantly greater than zero (right-tailed). Results were Bonferonni corrected for 17 time bins, two brain structures, and two behavioral conditions: *alpha* = 0.000735. P-values are shown directly below each time bin in both (a) and (b). Time bins where pFeeder was significantly greater than zero are indicated by blue and pink shading, for vStr and OFC, respectively. vStr showed greater decoding to the chosen feeder site nearly one second before the MidPoint time. OFC showed values significantly different from zero after the MidPoint. **(b)** Chosen side minus unchosen side decoding for VTE laps only (n=1066). The green line marks the TurnAround. Conventions are as in (a). For both structures, values were not greater than zero until after TurnAround. Significant time bins for vStr preceded those for OFC on both non-VTE laps and VTE laps.

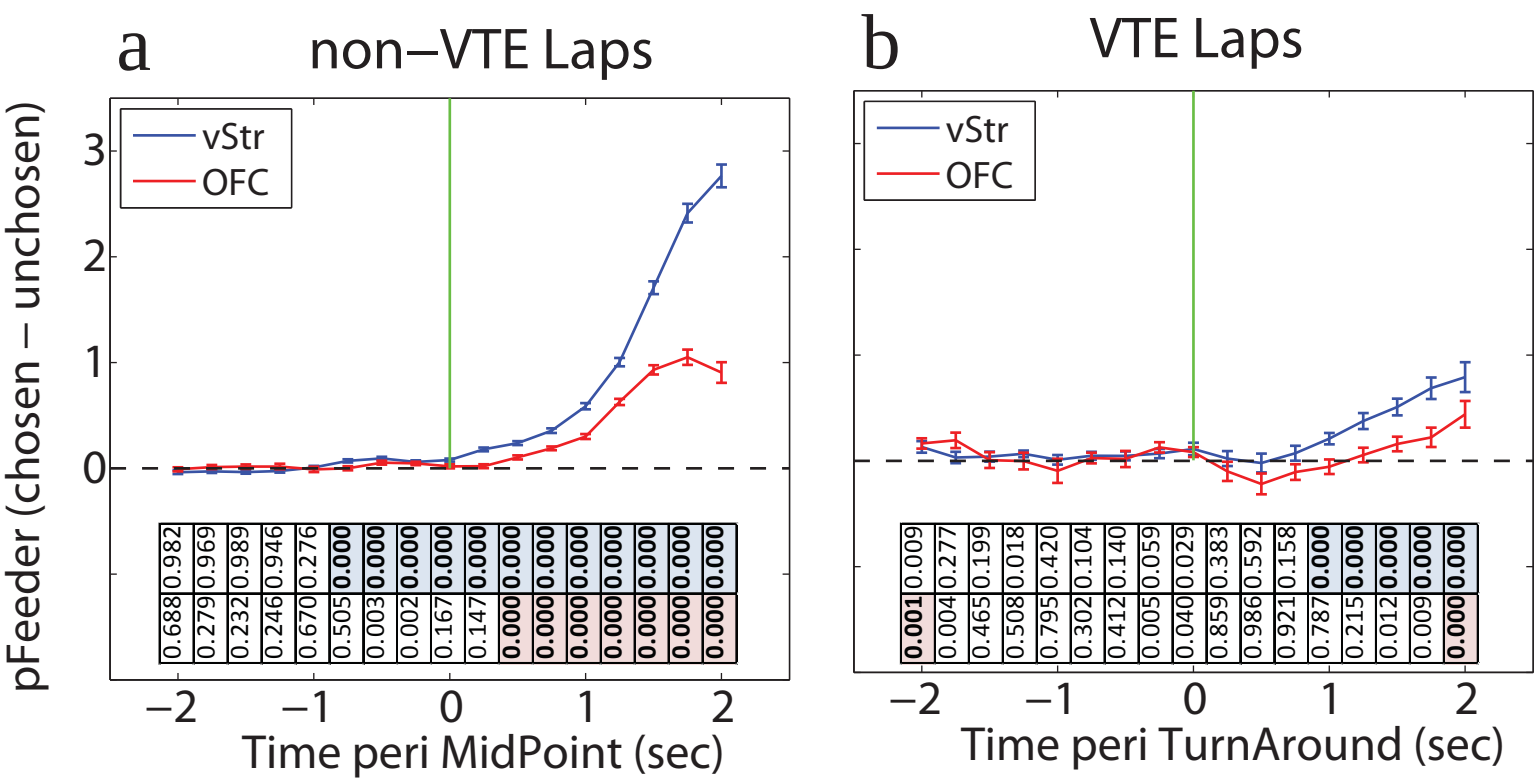
a
non–VTE Laps
vStr
OFC
pFeeder (chosen – unchosen)
3
2
1
0
0.688 0.279 0.232 0.246 0.670 0.505 0.003 0.002 0.167 0.147
0.982 0.969 0.989 0.946 0.276
0.000 0.000 0.000 0.000 0.000 0.000 0.000 0.000 0.000 0.000
−2 −1 0 1 2
Time peri MidPoint (sec)
b
VTE Laps
vStr
OFC
0.001 0.004 0.465 0.508 0.795 0.302 0.412 0.005 0.040 0.859
0.009 0.277 0.199 0.018 0.420 0.104 0.140 0.059 0.029 0.383 0.986 0.921 0.787 0.215 0.012 0.009
0.592 0.158
0.000 0.000 0.000 0.000 0.000
−2 −1 0 1 2
Time peri TurnAround (sec)

Figure S8: SPATIAL CONTROL for Fig 5. In order to control for potential spatial confounds, we recalculated the covert reward analyses using the expected firing rate of each cell given the spatial location of the animal. We first calculated the spatial tuning curve of each cell, and then substituted the average firing rate of the cell at the current location of the rat for the actual firing rate of the cell in the Bayesian decoding analysis. This removes any information not derived from the actual location of the rat and controls for any spatial differences in the location of the rat during the pass through the choice point. As in Figure 5, data was averaged within session (n = 85 sessions). Lines represent the average across sessions, with error bars representing the standard error (SEM). **(a)** Average feeder site decoding for vStr. VTE laps are aligned to the point of TurnAround and non-VTE laps are aligned to the MidPoint of the choice point trajectory. P-values are shown below each time bin as in Fig. 5. **(b)** Average feeder site decoding for OFC (n = 85 sessions). Conventions as in (a). Note that for both vStr and OFC, the value of *pFeeders* for VTE laps is even with or below that for non-VTE laps, indicating that the increases in VTE seen in Fig. 5 are not due to spatial position.

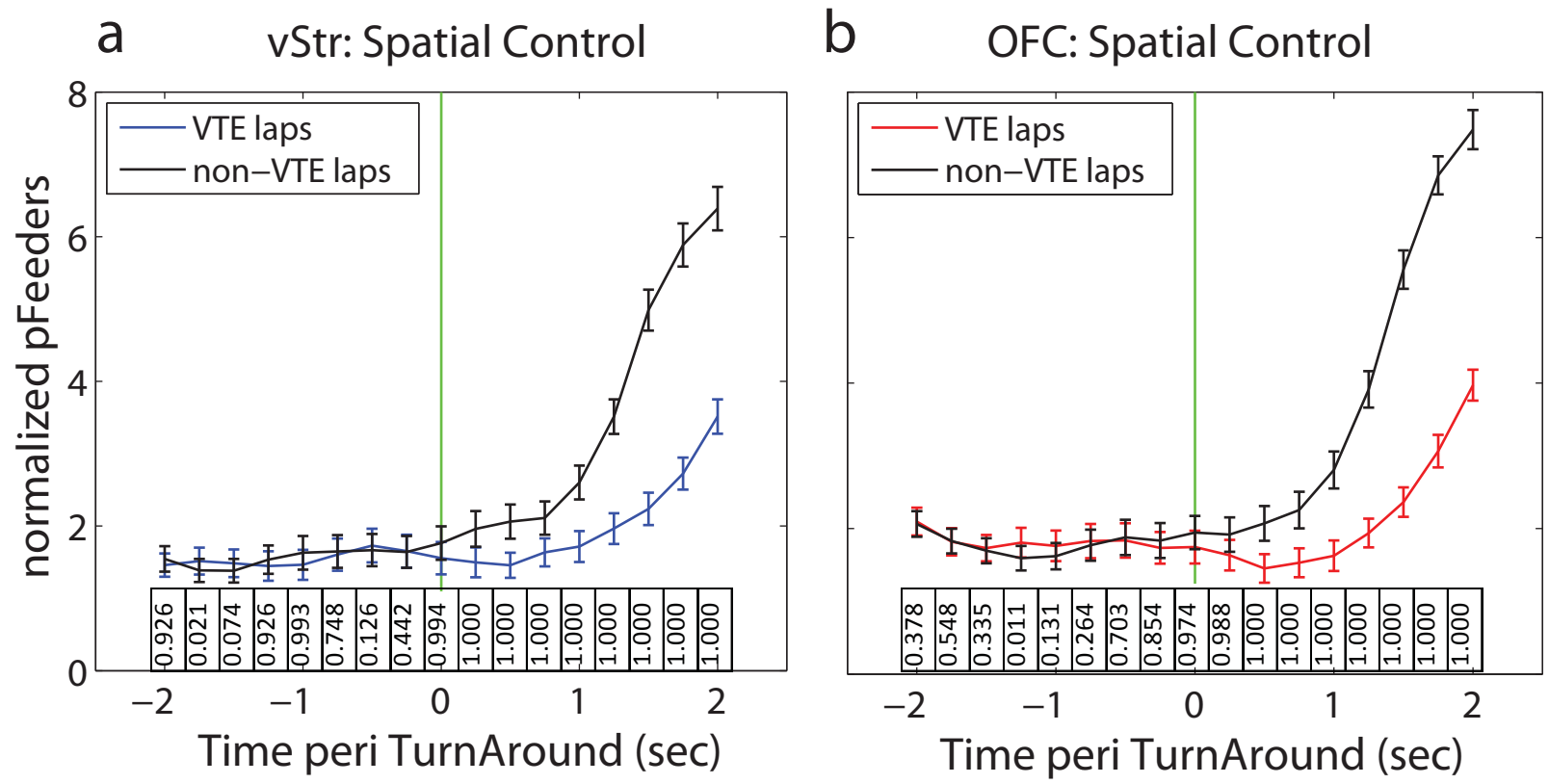
a
vStr: Spatial Control
VTE laps
non–VTE laps
normalized pFeeders
0
2
4
6
8
0.926
0.021
0.074
0.926
0.993
0.748
0.126
0.442
0.994
1.000
1.000
1.000
1.000
1.000
1.000
1.000
1.000
−2
−1
0
1
2
Time peri TurnAround (sec)
b
OFC: Spatial Control
VTE laps
non–VTE laps
0.378
0.548
0.335
0.011
0.131
0.264
0.703
0.854
0.974
0.988
1.000
1.000
1.000
1.000
1.000
1.000
1.000
−2
−1
0
1
2
Time peri TurnAround (sec)

Figure S9: SPATIAL CONTROL for Fig. 6. Same spatial control as above, but applied to the analysis from Fig. 6. **(a)** Decoding to the chosen feeder site minus decoding to the unchosen feeder site for non-VTE laps. The green line marks the MidPoint time. Values above the dotted line indicate greater decoding to the chosen feeder site. P-values are shown directly below each time bin in both (a) and (b). Time bins where vStr or OFC was significantly greater than zero (t-tests on each time bin—Bonferonni corrected—*alpha* = 0.000735) are indicated by blue and pink shading, for vStr and OFC, respectively. **(b)** Chosen side minus unchosen side decoding for VTE laps only. The green line marks the TurnAround. For both structures, and both conditions (non-VTE & VTE), values were not greater than zero until after TurnAround. Importantly, the emergence of significance for vStr before OFC in Fig. 6 is not seen here, indicating that the earlier timing seen in vStr in Fig. 6 is not due to spatial position.

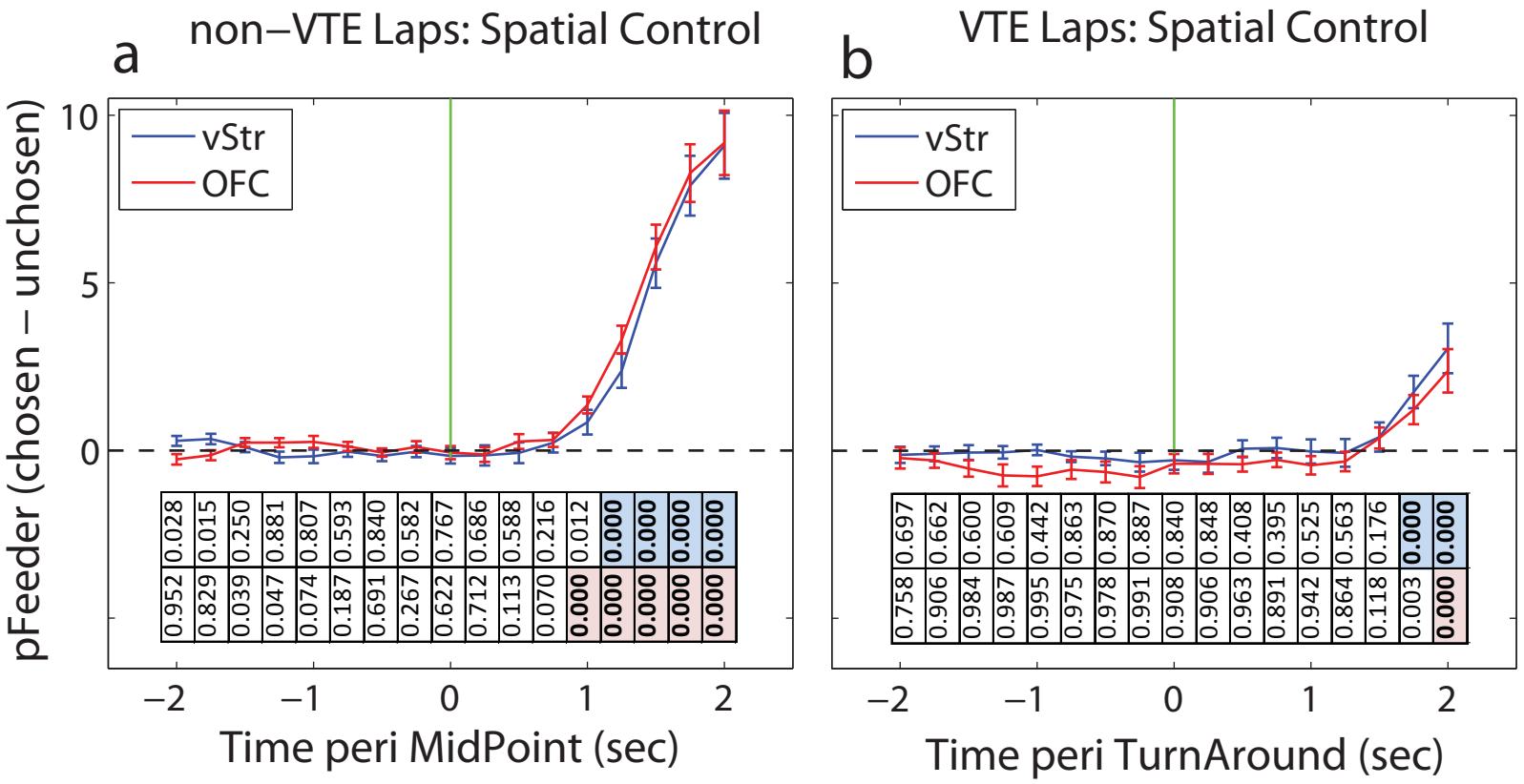
a
non−VTE Laps: Spatial Control
vStr
OFC
pFeeder (chosen − unchosen)
10
5
0
−2
−1
0
1
2
Time peri MidPoint (sec)
0.952 0.829 0.039 0.047 0.074 0.187 0.691 0.267 0.622 0.712 0.113 0.070 0.000 0.000 0.000 0.000 0.000
0.028 0.015 0.250 0.881 0.807 0.593 0.840 0.582 0.767 0.686 0.588 0.216 0.012 0.000 0.000 0.000 0.000
b
VTE Laps: Spatial Control
vStr
OFC
−2
−1
0
1
2
Time peri TurnAround (sec)
0.758 0.906 0.984 0.987 0.995 0.975 0.978 0.991 0.908 0.906 0.963 0.891 0.942 0.864 0.118 0.003 0.000
0.697 0.662 0.600 0.609 0.442 0.863 0.870 0.887 0.840 0.848 0.408 0.395 0.525 0.563 0.176 0.000 0.000